

Research Paper

# Bovine serum albumin aggravates macrophage M1 activation and kidney injury in heterozygous Klotho-deficient mice via the gut microbiota-immune axis

Lingyun Lai<sup>1\*</sup>, Yi Li<sup>2\*</sup>, Jianjun Liu<sup>3\*</sup>, Lei Luo<sup>2</sup>, Jianguo Tang<sup>3</sup>, Jun Xue<sup>1</sup>✉ and Te Liu<sup>4,5</sup>✉\*

1. Division of Nephrology, Huashan Hospital, Fudan University, Shanghai 200040, China.
2. Division of Nephrology, Shuguang Hospital, Shanghai University of Traditional Chinese Medicine, Shanghai 201203, China.
3. Trauma-Emergency & Critical Care Medicine Center, Shanghai Fifth People's Hospital, Fudan University, Shanghai 200240, China.
4. Shanghai Geriatric Institute of Chinese Medicine, Shanghai University of Traditional Chinese Medicine, Shanghai 200031, China.
5. Department of Pathology, Yale University School of Medicine, New Haven, Connecticut 06520, USA.

\*Co-first authors with equal contributions to this work.

✉ Corresponding authors: Prof. Jun Xue, Division of Nephrology, Huashan Hospital, Fudan University, Shanghai, China, 200040, Phone: 86-21-528877999; Fax: 86-21-52887799; E-mail: xuejun@fudan.edu.cn. Prof. Te Liu, Shanghai Geriatric Institute of Chinese Medicine, Shanghai University of Traditional Chinese Medicine, Shanghai, China, 200031, Phone: 86-21-64720010; Fax: 86-21-64720010; E-mail: 0721160004@mail.tongji.edu.cn.

© The author(s). This is an open access article distributed under the terms of the Creative Commons Attribution License (<https://creativecommons.org/licenses/by/4.0/>). See <http://ivyspring.com/terms> for full terms and conditions.

Received: 2020.11.25; Accepted: 2021.01.18; Published: 2021.02.02

## Abstract

Klotho expression abnormalities induces kidney injury and chronic kidney disease, however, the underlying mechanism remains unclear. Here, Klotho<sup>+/-</sup> mice and wild-type mice were treated with low-dose bovine serum albumin (BSA). Pathological examination demonstrated that the area of glomerular collagen deposition and fibrosis in BSA-Kl<sup>+/-</sup> mice was significantly larger than that in BSA-WT mice. The serum levels of superoxide dismutase, malondialdehyde, creatinine, and urea in BSA-Kl<sup>+/-</sup> mice were significantly increased. Sequencing of gut microbiota 16S rRNA v3-v4 region indicated that BSA-Kl<sup>+/-</sup> mice showed a significantly higher relative abundance of the genera *Dubosiella*, *Akkermansia*, *Alloprevotella*, and *Lachnospiraceae* and a significantly lower relative abundance of the genera *Allobaculum* and *Muribaculaceae* than BSA-WT mice. KEGG analysis revealed that the metabolic pathways of signal transduction, xenobiotic biodegradation and metabolism, and lipid metabolism increased significantly in BSA-Kl<sup>+/-</sup> mice. Flow cytometry showed that the proportion of CD68<sup>+</sup>/CD11b<sup>+</sup> cells in the peripheral blood was significantly higher in BSA-Kl<sup>+/-</sup> mice than that in BSA-WT mice. qPCR and western blot suggested that Klotho and Nrf2 expression in MΦ1 cells of BSA-Kl<sup>+/-</sup> mice was significantly decreased. Thus, the findings suggest during the immune activation and chronic inflammation induced by the gut microbiota imbalance in Klotho-deficient mice treated to BSA, disrupted expression of proteins in the Nrf2/NF-κB signaling pathway in monocyte-derived macrophage M1 cells leads to the aggravation of inflammation and kidney injury.

Key words: gut microbiota, macrophage M1, Klotho, Nrf2/NF-κB pathway, kidney injury

## Introduction

Chronic kidney disease affects approximately 10% of the global population and has a financial impact of approximately \$48 billion per year in the United States alone [1, 2]. Hypertension is an important risk factor for CKD, and approximately 85-90% of patients with CKD stage 3-5 have hypertension [1, 2]. Increasing evidence indicates an important role of the gut microbiota in the development of hypertension and CKD [1-3]. The

human gut microbiota comprises more than 100 trillion microbial cells, including aerobic and anaerobic species and gram-positive and gram-negative species [4]. The gut microbiota constantly communicates with vital organ systems of the host, such as the brain, bone marrow, vasculature, kidney, immune system, and autonomic nervous system [1, 5, 6]. Trimethylamine-N-oxide, short-chain fatty acids, and inflammatory factors derived from the gut

microbes may induce changes in arteries, kidneys, and blood pressure [4]. In addition, bacterial 16S rDNA amplification and DNA pyrosequencing suggest that the DNA of gut microbiota is present in the plasma of CKD patients on chronic hemodialysis [7, 8], and the levels of bacterial DNA is correlated with increased plasma inflammatory marker levels [7, 8]. Our previous study revealed that ranitidine and finasteride inhibit the synthesis and release of trimethylamine N-oxide and mitigate its cardiovascular and kidney damage through modulating gut microbiota [9]. Indoxyl sulfate is a typical uremic toxin that is not efficiently removed by hemodialysis; modulation of indoxyl sulfate production in the gut microbiota is a promising strategy for decreasing indoxyl sulfate concentration, thus delaying CKD progression [10]. Therefore, exploring the relationship between gut microbiota and kidney disease important for the development of effective therapeutic drugs.

Klotho (*KL*) was initially identified as an anti-aging gene, mainly expressed in the kidney and cerebral choroid plexus [11-16]. Human *KL* gene encodes  $\alpha$ -Klotho, a multifunctional protein that regulates the metabolism of phosphate, calcium, and vitamin D and acts as a hormone [14, 17-22]. A human *KL* gene point mutation is associated with hypertension and kidney disease, suggesting that *KL* maintains normal kidney function. *Kl* overexpression in mice prolongs their life [11, 13, 19, 23]. *KL* gene knockout accelerates aging and shortens the life span [18-22]. The *KL* gene encodes three protein forms: full-length transmembrane *KL*, truncated soluble *KL*, and secretory *KL* (s*KL*). Soluble *KL* is produced by releasing the extracellular domain of transmembrane *KL*, whereas s*KL* is produced by selective RNA splicing [12-14, 24]. s*KL* secreted from the cells is found in blood, urine, and cerebrospinal fluid [12-14]; it is an endocrine factor that targets distal organs and regulates the activity of cell surface ion channels and transporters [12-14]. Klotho deficiency is closely associated with kidney disease. In patients with CKD stages 1-5, the combination of higher C-terminal fibroblast growth factor 23 and lower s*KL* levels were associated with adverse clinical outcomes [25]. High plasma phosphate and Klotho deficiency contribute to kidney epithelial senescence and kidney fibrosis, an important pathological feature in the aging kidney and chronic kidney disease [26]. In *Kl*<sup>-/-</sup> mice, severe skeletal muscle atrophy was observed, and autophagy-lysosome pathway was activated. The signal transduction activity of mTOR was inhibited, likely due to the lack of essential amino acids in *KL*-deficient glomeruli [18]. Chen and others reported that RGFP966, a selective inhibitor of histone

deacetylase 3 (HDAC3), derepressed Klotho and alleviated renal fibrotic injuries in mice with unilateral ureter obstruction and aristolochic acid nephropathy [27]. HDAC3 overexpression or inhibition in renal epithelia was inversely related to Klotho levels, and HDAC3 was inducibly associated with transcriptional regulators NCoR and NF- $\kappa$ B and bound to Klotho promoter in fibrotic kidney, reinforcing that aberrant HDAC3 targets Klotho and inhibits its transcription in renal fibrosis [27]. Diabetic nephropathy is also associated with decreased renal klotho expression and renal mitochondrial injury, and klotho exerts a mitochondrial effect on renal mitochondria via LKB1-AMPK-PGC1 $\alpha$  expression and ameliorates diabetic nephropathy [28]. Moreover, Klotho alleviates kidney and cardiac injury by inactivating NF- $\kappa$ B signaling and promoting macrophage M2 polarization, potentially mitigating indoxyl sulfate-induced heart failure and chronic kidney disease or acute kidney injury [29]. Thus, Klotho is closely associated with inflammation, renal fibrosis, and kidney disease.

Nuclear factor erythroid 2-like 2 (NFE2L2, also named Nrf2) is a redox sensitive transcription factor that regulates the basal and inducible expression of an array of antioxidant and detoxifying enzymes, including glutamate cysteine ligase, quinone oxidoreductase 1 and heme oxygenase-1. Under non-stimulated conditions, Nrf2 is rapidly degraded in the cytosol through ubiquitination mediated by Keap1 [30, 31]. The current study showed that NF- $\kappa$ B activation might also be required for Nrf2 signaling in response to redox sensitive or inflammatory triggers [30, 32]. Sayan Ghosh and their group found that significant alterations in Nrf2-dependent cellular redox status, coupled with altered autophagy and increased apoptosis were noticed in the hippocampus of LPS-exposed mice [33]. And they found that modulating the activity of Nrf2/NF- $\kappa$ B signaling pathway could achieve anti-inflammatory and antioxidant properties effect [33]. Moreover, Ulrike A Köhler et al found that loss of either Nrf2 or NF- $\kappa$ B/RelA had only a minor effect on liver homeostasis, but the double knockout mice spontaneously developed liver inflammation and fibrosis. So, they suggested that functional cross-talk of Nrf2 and NF- $\kappa$ B/RelA in hepatocytes protected the liver from necrosis, inflammation and fibrosis [34]. A series of studies have pointed out that Nrf2/NF- $\kappa$ B signaling pathway is closely related to inflammatory response.

In the present study, we investigated whether in Klotho-deficient mice treated with BSA, the changes in intestinal microflora structure and effects on the immune system induce kidney damage and CKD.

## Material and methods

### Mouse model

$\alpha$ -Klotho heterozygous hypomorphic male mice (Klotho<sup>-/+</sup>, KL<sup>-/+</sup>), as previously described [35] were used in this study. A total of 20, specific-pathogen-free-grade, 6–8-week-old, male mice (Klotho<sup>-/+</sup> [n = 10] and WT C57BL/6 [n = 10]; average weight = 28 ± 5 g) were purchased from Shanghai Model Organisms Company (Modelorg, Shanghai, China; License number: SCXK (Shanghai) 2019-0004). After 1 week of adaptive feeding, as described in previous reports [36], 5 and 1 mg/g body weight BSA (A-7906, Sigma-Aldrich, St. Louis, USA) was administered to all mice by intraperitoneal gavage for the first 2 days. Then, for 3 weeks, 1.5 mg/g body weight BSA was administered by gavage. This study was approved by the ethics committee of the Shanghai Geriatric Institute of Chinese Medicine (SHAGESYDW201908). All experiments conformed to the experimental animal regulations of the Ministry of Science and Technology.

### Hematoxylin-eosin staining

All fresh tissues were fixed in 4% paraformaldehyde (Sigma-Aldrich) for 30 min at room temperature. Tissues were dehydrated using an ethanol gradient, embedded in paraffin, sectioned (6  $\mu$ m thickness), and dewaxed by immersion in xylene. Tissue sections were stained with hematoxylin-eosin (Sigma-Aldrich), permeabilized with xylene (Sigma-Aldrich), and mounted in neutral resin (Sigma-Aldrich) [35].

### Masson staining

The sections were washed with double-distilled water for 5 min and then stained with hematoxylin (Beyotime Biotechnology) for 5–10 min, followed by thorough rinsing with water. The sections were counterstained with Masson's ponceau acid fuchsin solution (Beyotime Biotechnology) for 6–10 min and then rinsed with 2% ice-cold aqueous acetic acid (Beyotime Biotechnology) for 5 s. The sections were differentiated for 3–5 min with 1% aqueous phosphomolybdic acid (Beyotime Biotechnology), stained by direct immersion in aniline blue for 5 min, and then washed with 0.2% aqueous glacial acetic acid (Beyotime Biotechnology) for several seconds. The stained sections were cleared, sealed, and photographed [9]. The quantitative statistical method of collagen area from masson staining: Collagen area fraction (%) = (MASSON staining collagen positive area / total area) \* 100%".

### Periodic acid-Schiff (PAS) staining

Briefly, the sections were washed with double-distilled water for 5 min and then stained with 10 g/L Periodate (Beyotime Biotechnology) for 20 min, followed by thorough rinsing with water. The sections were counterstained with Schiff solution (Beyotime Biotechnology) for 60 min and then rinsed with sulfite (Beyotime Biotechnology) for 3 times, followed by thorough rinsing with water. Next, the sections were counterstained with Methyl green solution (Beyotime Biotechnology) for 20 min, followed by thorough rinsing with water. The stained sections were cleared, sealed, and photographed.

### The quantitative real-time reverse transcription PCR (qRT-PCR) assay

Briefly, total cellular RNA was extracted using the Trizol Reagent (Invitrogen, Waltham, MA, USA) according to the manufacturer's protocol. The RNA was then reverse-transcribed into cDNA using a ReverTra Ace- $\alpha$  First Strand cDNA Synthesis Kit (TOYOBO, Osaka, Japan). cDNA was then amplified using quantitative real-time PCR (qPCR). QPCR was conducted using a RealPlex4 real-time PCR detection system from Eppendorf Co. Ltd (Hamburg, Germany), with the SyBR Green RealTime PCR Master Mix and detection dye (TOYOBO). QPCR amplification was performed over 40 cycles. The qPCR cycle consisted of denaturation at 95 °C for 15 s and annealing at 58 °C for 45 s. The target cDNA was evaluated by relative quantification. A comparative cycle threshold (Ct) method was used to determine the gene expression relative to a control (calibrator, 18S rRNA) and steady-state mRNA levels were reported as an n-fold difference relative to that of the calibrator. For each sample, the marker gene Ct values were normalized using the formula  $\Delta Ct = Ct_{\text{genes}} - Ct_{18S \text{ rRNA}}$ . To determine the relative expression levels, the following formula was used:  $\Delta\Delta Ct = \Delta Ct_{\text{treated\_group}} - \Delta Ct_{\text{control\_group}}$ . Three biological replications were performed for each reaction. The 2- $\Delta\Delta Ct$  method was applied to measure the relative marker expression. The internal control, 18S rRNA, served as a normalizer. The sequences of the real-time PCR primers were as follows: KI-F: ACTACGTTCAA GTGGACACTACT; KI-R: GATGGCAGAGAAATCA ACACAGT; Nfkb1-F: ATGGCAGACGATGATCCC TAC; Nfkb1-R: TGTTGACAGTGGTATTTCTGGTG; Ifng-F: ATGAACGCTACACACTGCATC; Ifng-R: CCATCCITTTGCCAGTTCCTC; Tnf-F: CCTGTAGC CCACGTCGTAG; Tnf-R: GGGAGTAGACAAGGTA CAACCC; Il1b-F: GAAATGCCACCTTTTGACAGTG; Il1b-R: TGGATGCTCTCATCAGGACAG; Nfe2l2-F: TCTTGGAGTAAGTCGAGAAGTGT; Nfe2l2-R: GTT GAAACTGAGCGAAAAAGGC; 18S rRNA-F: CAGC

CACCCGAGATTGAGCA; 18S rRNA-R: TAGTAGCGACGGGCGGTGTG.

### Kidney function parameter analysis

Plasma urea level was detected with a urea assay kit (DIUR-500; BioAssay Systems, Hayward, CA, USA). Plasma and urinary creatinine levels were detected using a creatinine assay kit (DICT-500; BioAssay Systems). Urinary albumin concentration was measured with a mouse-specific microalbuminuria ELISA kit (Albuwell M; Exocell, Philadelphia, PA, USA). All kidney function parameters were measured according to manufacturers' instructions [16].

### Gut microbiota analysis

As described in previous studies [37, 38], fresh fecal samples were collected during the last 5 days of the experiment to analyze the gut microbiota. Bacterial genomic DNA was extracted from frozen samples stored at  $-80^{\circ}\text{C}$ . The V3 and V4 regions of the 16S rRNA gene were amplified by PCR using specific bacterial primers (F primer: 5'-ACTCCTACGGGAGG CAGCA-3'; R primer: 5'-GGACTACHVGGGTWCT AAT-3'). High-throughput pyrosequencing of the PCR products was performed on an Illumina MiSeq platform at Biomarker Technologies Co. Ltd. (China). The raw paired-end reads from the original DNA fragments were merged using FLASH32 and assigned to each sample, according to the unique barcodes. QIIME [39] (version 1.8.0) UCLUST [40] software was used based on 97% sequence similarity. The tags were clustered into operational taxonomic units. The alpha diversity index was evaluated using Mothur software (v.1.30). The diversity index was compared among samples by standardizing the number of sequences contained in each sample. Operational taxonomic unit rank curves, rarefaction curves, and Shannon curves were constructed, and Shannon, Chao1, Simpson, and abundance-based coverage estimator indexes were calculated. For beta diversity analysis, heatmaps of RDA-identified key operational taxonomic units, principal coordinate analysis [41], non-metric multidimensional scaling [42], and unweighted pair-group method with arithmetic mean were obtained using QIIME. The linear discriminant analysis-effect size (LEfSe) method was used for the quantitative analysis of biomarkers in each group. The linear discriminant analysis-effect size (linear discriminant analysis threshold  $>4$ ), non-parametric factorial Kruskal-Wallis sum-rank test, and unpaired Wilcoxon rank-sum test were performed to identify the taxa with significantly different abundance [43, 44].

### Western blot

Western blot analysis of protein expression was performed according to a previously described method [35]. In brief, total protein lysates were subjected to 12% sodium dodecyl sulfate polyacrylamide gel electrophoresis and transferred onto hybrid polyvinylidene fluoride membranes (Millipore, Bedford, USA). After blocking, the polyvinylidene fluoride membranes were washed four times for 15 min with Tris-buffered saline containing Tween-20 at room temperature, followed by incubation with the primary antibody (Table S2). Following extensive washing, membranes were incubated with the secondary antibody (Table S2) for 1 h. After washing, the immunoreactivity was visualized by enhanced chemiluminescence using an ECL kit (Perkin-Elmer Life Science, Norwalk, USA).

### Superoxide dismutase assay

The superoxide dismutase assay was performed using the SOD activity assay kit (Beyotime, Shanghai, China) according to the manufacturer's instructions [35]. In brief, 200  $\mu\text{L}$  of the sample lysate was added to  $1 \times 10^6$  cells/mL and was thoroughly mixed by pipetting. The mixture was centrifuged at  $12,000 \times g$  for 5 min at  $4^{\circ}\text{C}$ , and the supernatant was collected. The WST-8/enzyme working solution was prepared by thoroughly mixing 151  $\mu\text{L}$  of superoxide dismutase assay buffer, 8  $\mu\text{L}$  of WST-8, and 1  $\mu\text{L}$  of enzyme solution. A concentration gradient of superoxide dismutase standard solutions was prepared (100 U/mL, 50 U/mL, 20 U/mL, 10 U/mL, 5 U/mL, 2 U/mL, and 1 U/mL) and tested simultaneously with the samples. Twenty microlitres of the cell lysis supernatant and standard solutions were added to 160  $\mu\text{L}$  of freshly prepared WST-8/enzyme working solution and 20  $\mu\text{L}$  of reaction initiation solution, respectively. After thorough mixing, the samples were incubated at  $37^{\circ}\text{C}$  for 30 min. The absorbance was measured at 450 nm.

### Flow cytometry analysis

Mouse peripheral blood mononuclear cells (PBMCs) from each group were suspended ( $1 \times 10^6$  cells/mL) and stained with the primary antibodies (Table S2) on ice in Dulbecco's phosphate-buffered saline containing 10% BSA. Staining with an isotype control antibody (mouse IgG1-FITC, mouse IgG1-PE; Invitrogen, eBioscience™, Shanghai, China) was used to correct for non-specific binding. Antibody staining was analyzed by fluorescence correlation microscopy using a FACS Aria (Quanta SC, Beckman Coulter INC) [35].

## Statistical analysis

Each experiment was performed as least thrice; data are expressed as mean  $\pm$  standard error where applicable; differences were evaluated with Student's t-test. A  $P$  value  $<0.05$  was considered statistically significant.

## Results

### Bovine serum albumin caused significantly more kidney damage in $Kl^{-/+}$ mice than in WT mice

Hemoxilin-eosin, Masson, and periodic acid-Schiff staining showed that after BSA treatment,  $Kl^{-/+}$  mice (BSA- $Kl^{-/+}$ ) showed significantly higher renal mesangial proliferation, and significantly larger area

of glomerular collagen deposition, and fibrosis than WT mice (BSA-WT) (Fig. 1A-D). Moreover, the peripheral blood levels of superoxide dismutase (SOD) in BSA- $Kl^{-/+}$  mice were significantly lower than it in BSA-WT mice (Fig. 1E). However, the peripheral blood levels of malondialdehyde (MDA) in BSA- $Kl^{-/+}$  mice were significantly higher than those in BSA-WT mice (Fig. 1E). In addition, BSA- $Kl^{-/+}$  mice significantly higher levels of peripheral blood creatinine and urea and significantly lower levels of urinary creatinine than BSA-WT mice (Fig. 1F). Western blot showed that Klotho expression in the kidney was significantly lower in BSA- $Kl^{-/+}$  mice than in BSA-WT mice (Fig. 1G). The results indicate that, after BSA treatment,  $Kl^{-/+}$  mice showed a significantly greater degree of kidney damage than WT mice.

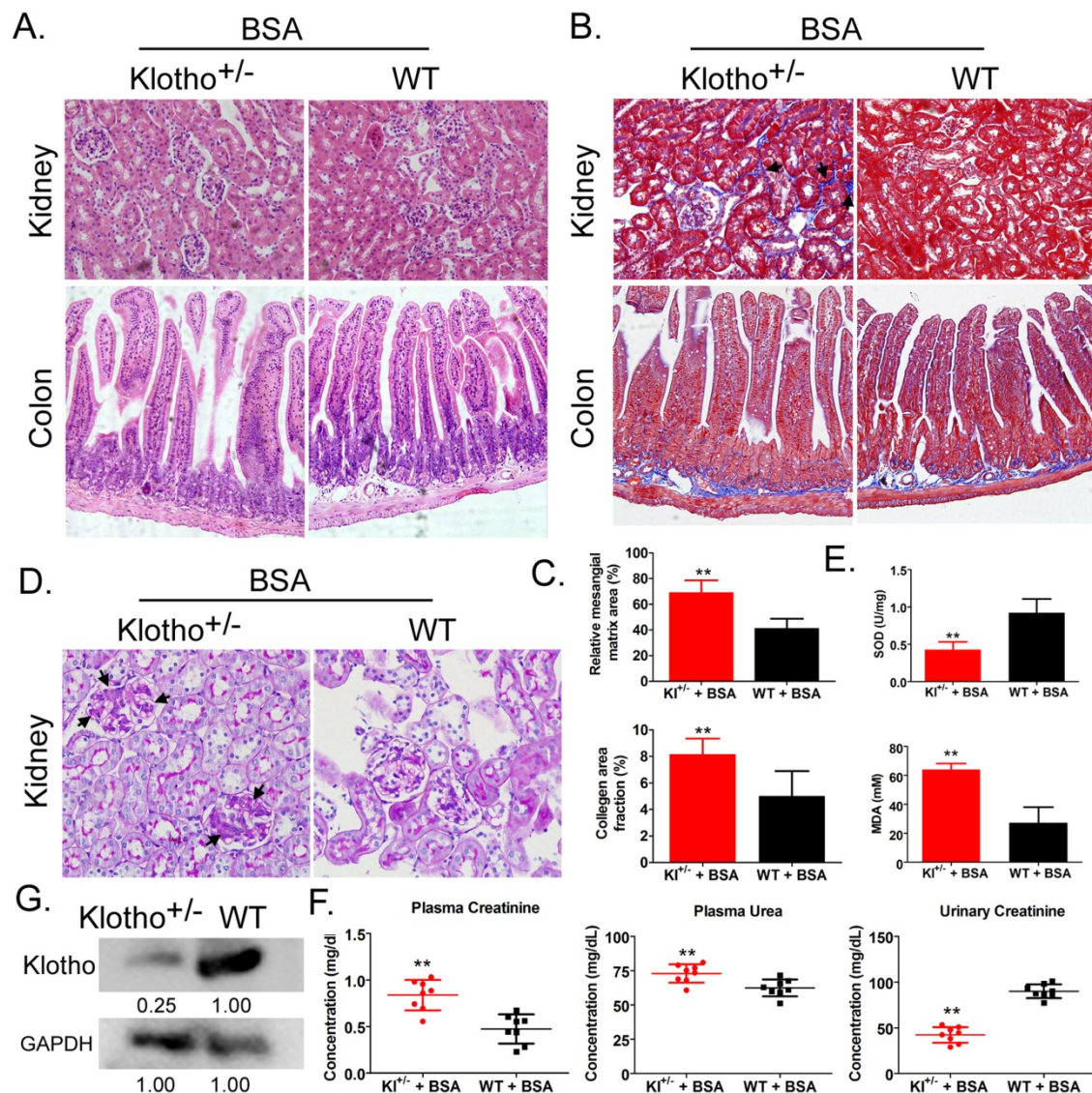


**Figure 1. Bovine serum albumin (BSA)-induced kidney injury in mice.** (A) Hematoxylin and eosin staining. Magnification 200 $\times$ . (B) Masson staining. Magnification 200 $\times$ . The arrow indicated the collagen deposition sites. (C) Comparisons of mesangial matrix area and collagen area fraction of kidney tissues in BSA-treated Klotho-deficient and wild-type mice. \*\* $p < 0.01$  (t test);  $n = 4$ . (D) Periodic acid-Schiff staining results. Magnification 200 $\times$ . The arrow indicated the mesangial hyperplasia sites. (E) Results of serum superoxide dismutase and malondialdehyde assays of BSA-treated Klotho-deficient and wild-type mice. \*\* $p < 0.01$  (t test);  $n = 4$ . (F) Creatinine and urea in serum and urea in urine in BSA-treated Klotho-deficient and wild-type mice. \*\* $p < 0.01$  (t test);  $n = 4$ . (G) Western blot of Klotho in the kidney tissue of BSA-treated Klotho-deficient and wild-type mice.

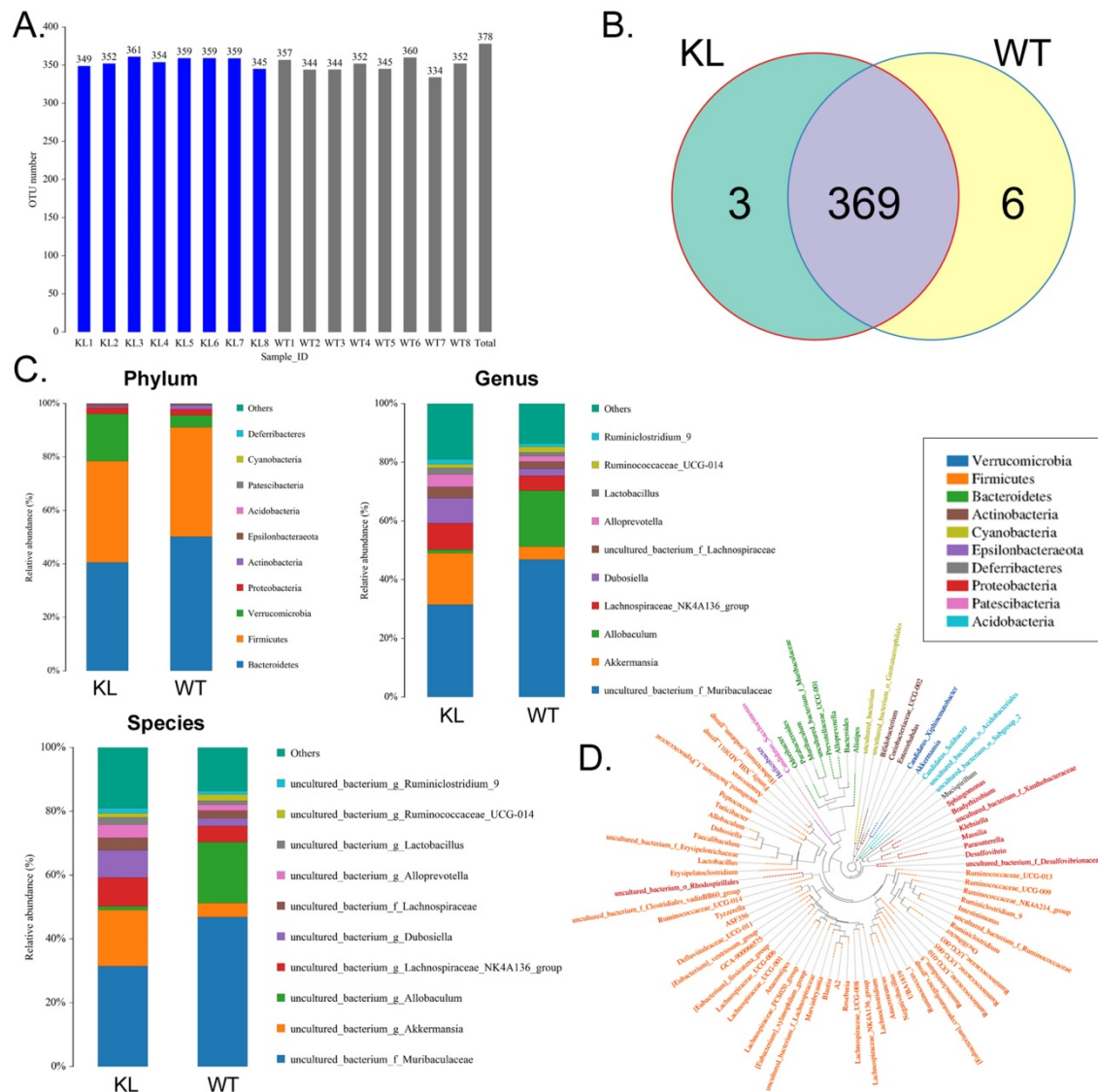


**Figure 2. Analysis of operational taxonomic units.** (A) Number of operational taxonomic units. (B) Venn diagram of operational taxonomic units. (C) Gut microbiota clustering and species distribution. (D) Species phylogenetic tree.

### Bovine serum albumin disrupts the balance of intestinal bacteria distribution and metabolism in KI<sup>-/+</sup> mice

The fecal samples of BSA-treated KI<sup>-/+</sup> mice and WT mice were processed and used for high-throughput sequencing of bacterial 16s rRNA v3-v4 regions to assess the specific composition and distribution of gut microbiota. Sequencing of 16 samples yielded 1,259,070 paired reads, producing 1152150 clean tags after joining and filtering the reads. Each sample produced at least 63,287 clean tags, producing an average of 72,009 clean tags (Table S1). Using QIIME (version 1.8.0) UCLUST software, tags were clustered into operational taxonomic units based on 97% similarity. The KI<sup>-/+</sup> and WT groups showed no significant difference in the number of operational taxonomic units (Fig. 2A). They had 369 operational

taxonomic units overlapping; the KI<sup>-/+</sup> group showed three unique operational taxonomic units, whereas WT has six unique operational taxonomic units (Fig. 2B). By comparing the sequence of the operational taxonomic units to a microbial reference database, each operational taxonomic unit can be assigned to a species. The community composition of each sample was also characterized. QIIME software was used to generate the species abundance at different levels of classification (Kingdom, Phylum, Class, Order, Family, Genus, and Species). Using R language tools, the community structure of the samples at different classification levels was determined. Phylum-level analysis showed that the KI<sup>-/+</sup> group mice showed a significantly higher relative abundance of phylum Verrucomicrobia and significantly lower relative abundance of phylum Bacteroidetes than the control group mice.

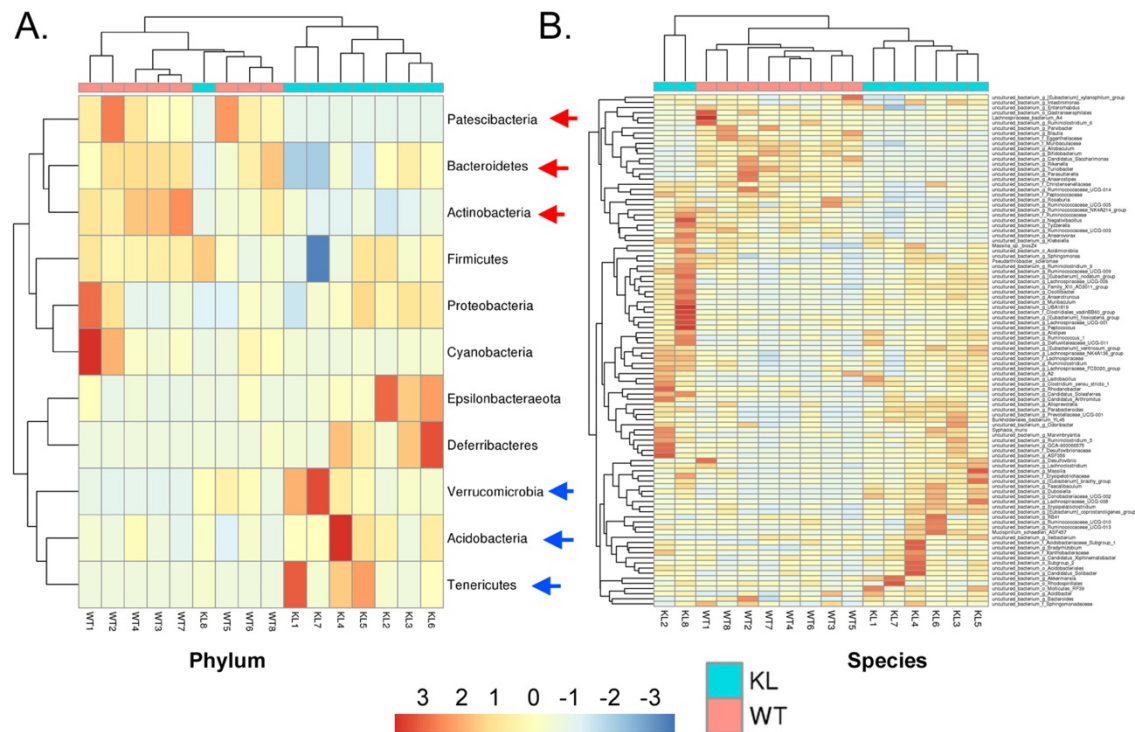


**Figure 3.** Heat map of species richness clustering at the level of: (A) Phylum; (B) Species.

Genus-level analysis showed that the  $Kl^{-/+}$  group mice showed a significantly higher relative abundance of the genera *Dubosiella*, *Akkermansia*, *Alloprevotella*, and *Lachnospiraceae* and significantly lower relative abundance of the genera *Allobaculum* and *Muribaculaceae* than the control group mice. Species-level analysis showed that the  $Kl^{-/+}$  group mice showed a significantly higher relative abundance of species belonging to the genera *Lachnospiraceae*, *Dubosiella*, *Alloprevotella*, *Akkermansia* microbes increased significantly, and a significantly lower relative abundance of species belonging to the genera *Allobaculum* and *Muribaculaceae* than the control group mice (Fig. 2C-D). Cluster analysis showed that the intestinal microbial diversity of the superphylum Patescibacteria, especially the phyla Bacteroidetes and Actinobacteria, was significantly lower and that of the phyla Verrucomicrobia, Acidobacteria, and Tenericutes was significantly higher in the  $Kl^{-/+}$  group mice than in the control group mice (Fig. 3).

Alpha diversity analysis found that rank-abundance curve showed a flat curve, suggesting a highly homogeneous species composition (Fig. 4A); Shannon curves tended to be flat, indicating that sequencing data quantity was sufficiently large; thus, the number of operational taxonomic unit species does not increase with the increasing quantity of sequencing data (Fig. 4B). Rarefaction curves were

smooth, indicating that sample sequences were complete and data analysis could be performed (Fig. 4C). Beta diversity analysis using the Bray-Curtis algorithms found differences in the microbial flora between groups. The analysis mainly includes the principal coordinate analysis, principal component analysis, and non-metric multidimensional scaling. According to the above analyses, microbial communities in the  $Kl^{-/+}$  and WT group samples show obvious differences of the distribution of group manager namely  $Kl^{-/+}$  group of microorganisms and WT group shall form a separate community (Fig. 5A). Unweighted pair-group method with arithmetic mean sample hierarchy clustering analysis results suggest that  $Kl^{-/+}$  and WT groups show a low homology of the gut microbiota, and there was no close genetic association (Fig. 5B-5D).

In addition, the line discriminant analysis (LDA) effect size was used to identify each species of the gut microbiota as important biomarkers; species of LDA scores  $>4$  are considered to be important biological markers. Cladogram analysis and LDA score distribution indicate that in the  $Kl^{-/+}$  group, a significantly high number of microorganisms belonging to phylum Verrucomicrobia, class Verrucomicrobiae, order Verrucomicrobiales, family *Akkermansiaceae*, and genus *Akkermansia*; therefore, the unique advantages of microbial community is  $Kl^{-/+}$  group strains (Fig. 6A-C).

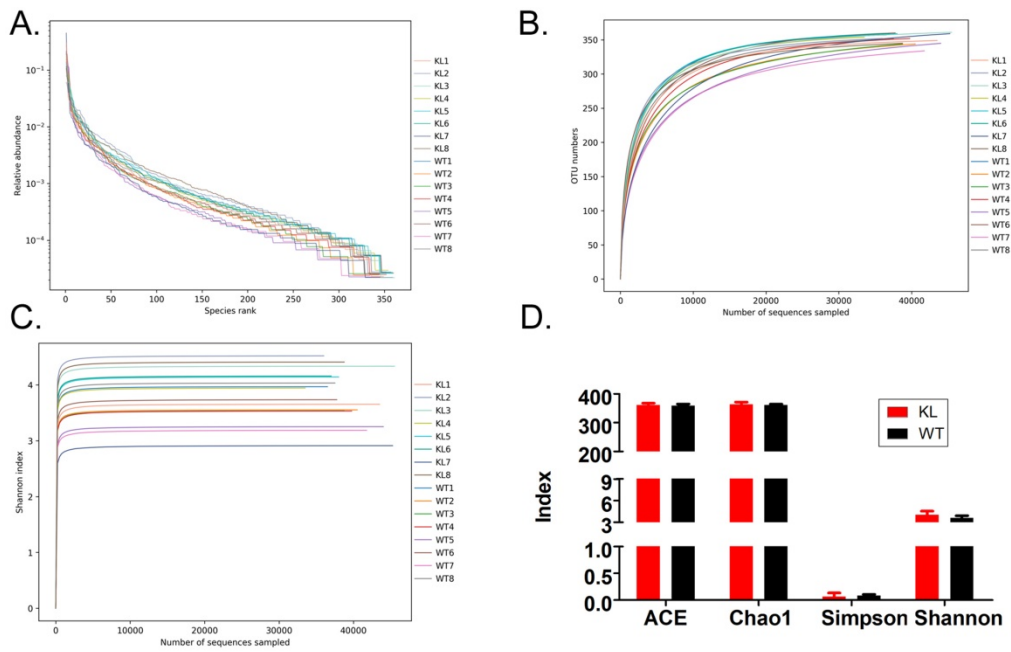


Figure 4. Alpha diversity analysis. (A) Rank abundance curve; (B) Rarefaction curve; (C) Shannon index curve; (D) Alpha diversity analysis.

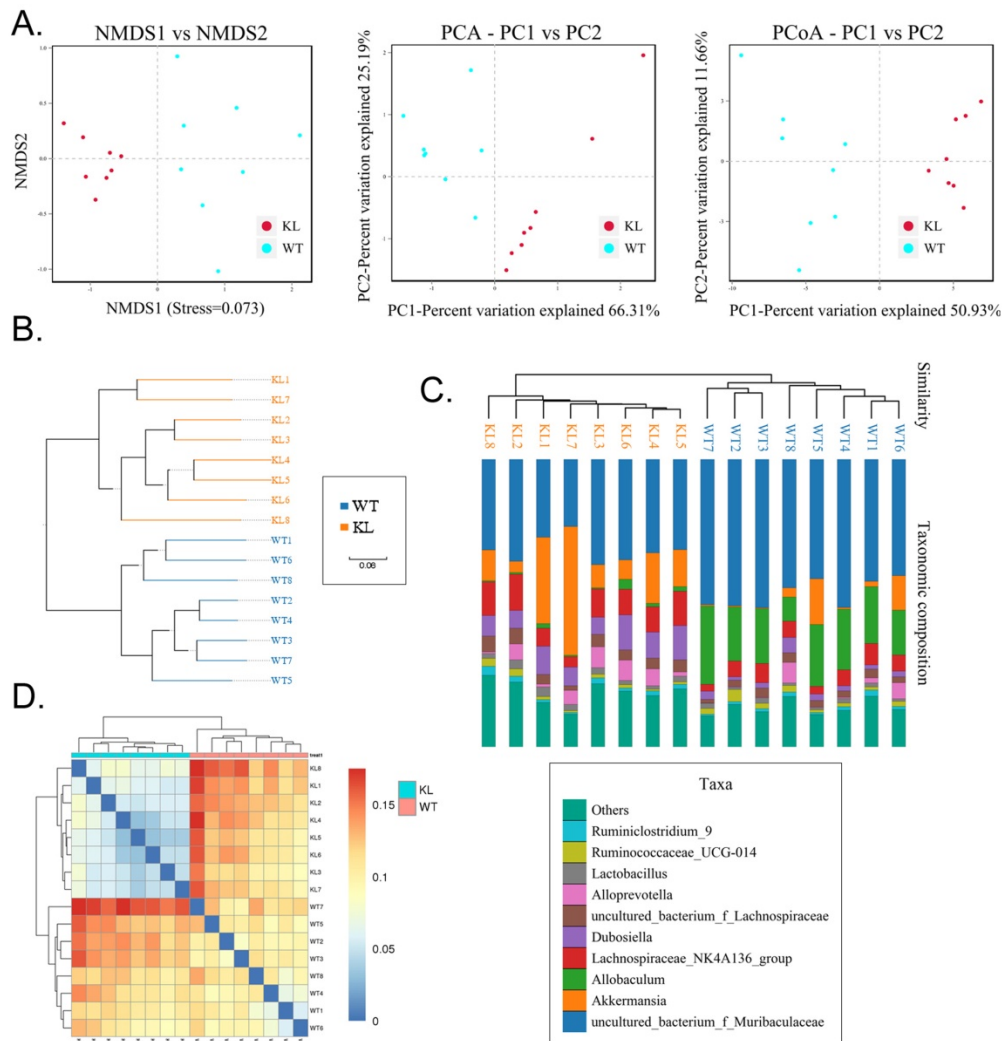
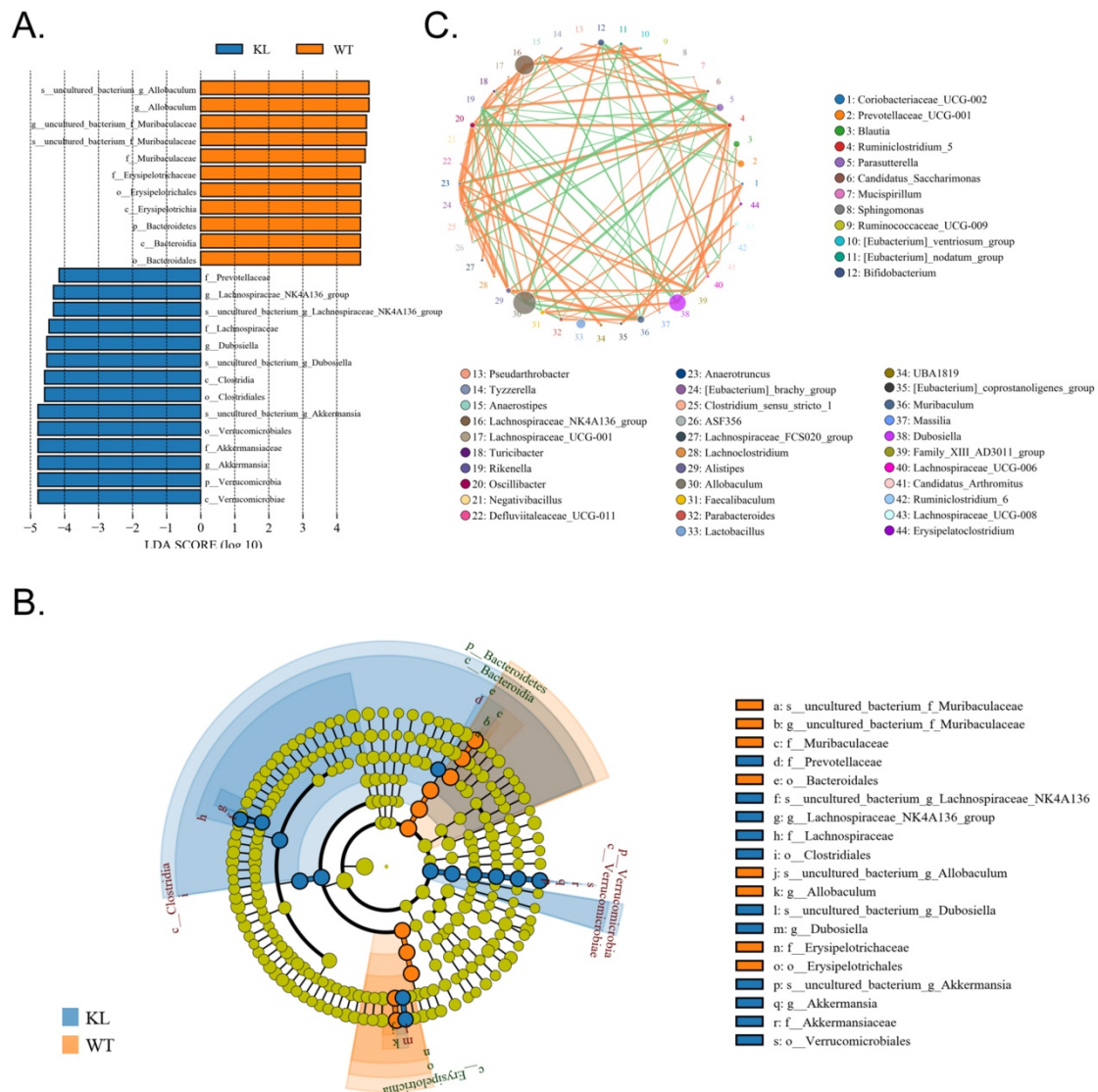


Figure 5. Beta diversity analysis. (A) Results of principal component analysis, principal coordinate analysis, and non-metric multidimensional scaling analysis. (B) Sample unweighted pair-group method with arithmetic mean clustering tree. (C) Combined drawing of clustering tree and histogram. (D) Heat map showing sample abundance.



**Figure 6. Significant difference analysis between groups.** (A) Value distribution histogram of line discriminant analysis effect size. (B) Results of species annotation were visualized using KRONA. (C) Species network at the genus level.

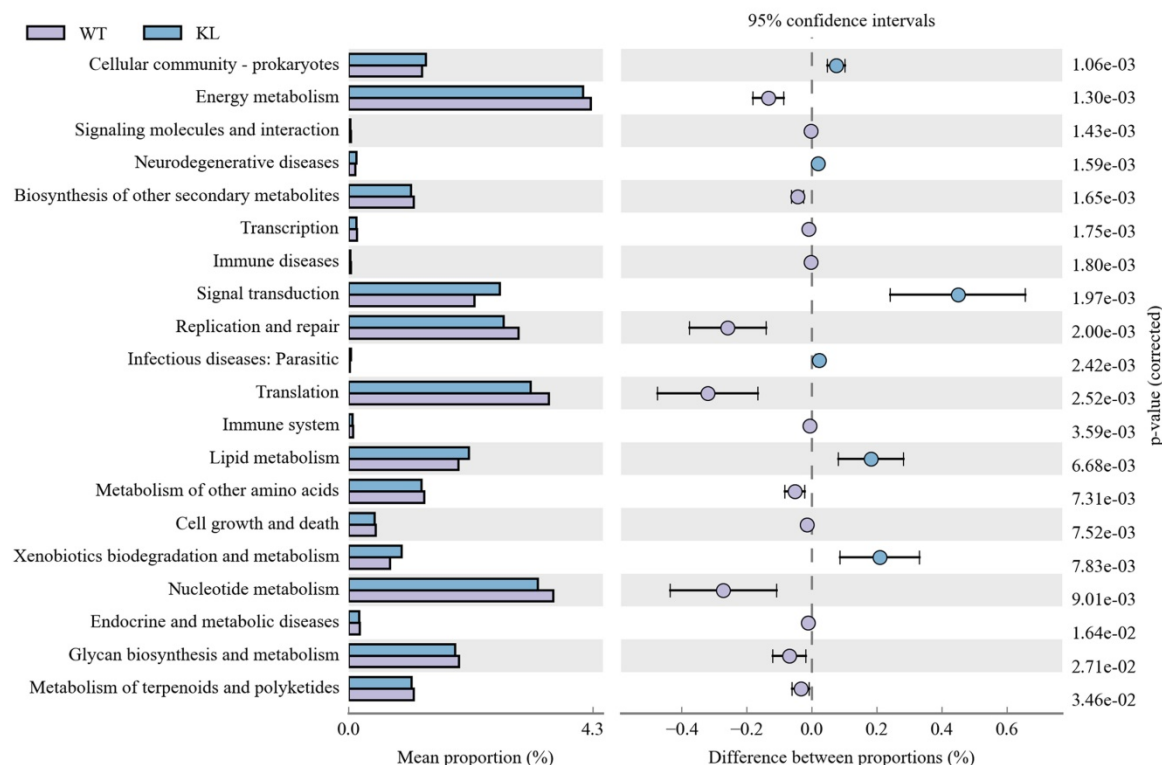
### Functional genes of gut microbes in KI<sup>-/+</sup> mice and the difference between the expression of metabolic pathway

Kyoto Encyclopedia of Genes and Genomes metabolic pathway analysis showed differences between samples from different groups in microbial community functional genes in metabolic pathways so as to explore the metabolic function change in different samples to adapt to environmental changes of (Table S5). Comparison of the KI<sup>-/+</sup> group with the WT group showed that the intestinal microbes of the KI<sup>-/+</sup> group have functional genes contributing to metabolic pathways in signal transduction (environmental information processing), xenobiotic biodegradation and metabolism (metabolism), lipid metabolism (metabolism), translation-based information processing, and nucleotide metabolism-

based information processing (such as replication and repair; Fig. 7A).

Analysis of clusters of orthologous groups of proteins showed that the distribution of the microbial homologous protein cluster belong to spend (Table S5). Results showed that the abundance of intestinal microbial proteins involved in metabolic pathways related signal transduction mechanisms (cellular the processes and signaling) and cell motility (cellular the processes and signaling) was significantly higher and that of intestinal microbial proteins involved in ribosomal structure and biogenesis (information storage and processing); replication, recombination, and repair (information storage and processing) was significantly lower in the KI<sup>-/+</sup> group than in the control group (Fig. 7B).

A.



B.

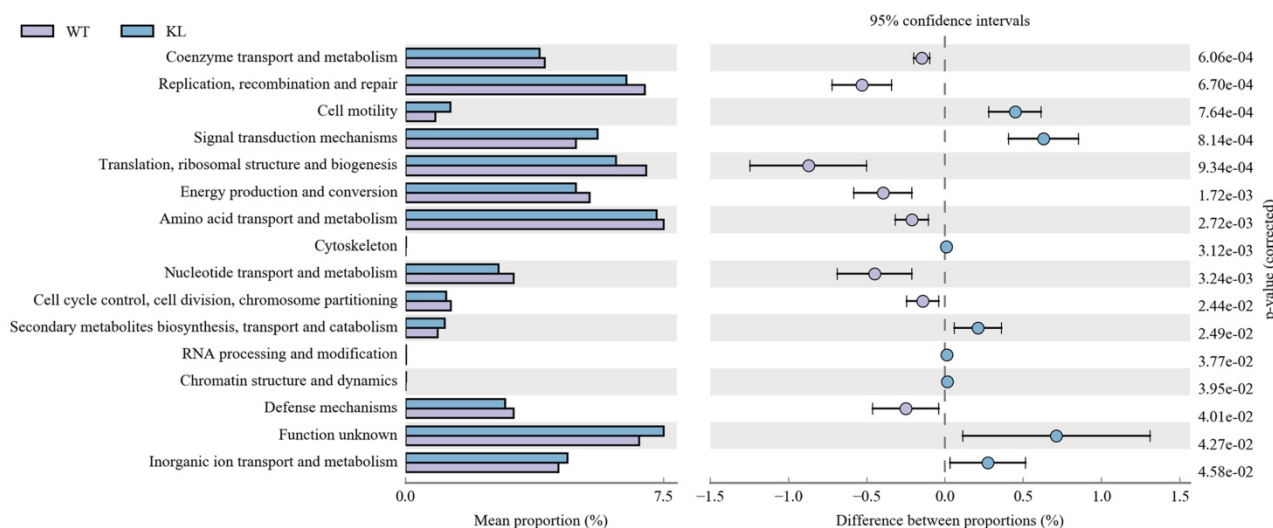


**Figure 7. Metabolic signaling pathways and protein differences in gut microbiota.** (A) Results of Kyoto Encyclopedia of Genes and Genomes metabolic pathway analysis. (B) Clusters of orthologous groups of proteins analysis of distribution and abundance of homologous protein clusters in gut microbiota.

### Bovine serum albumin treatment leads to unusually high number and activity of MΦ1 in KI<sup>-/+</sup> mice

Flow cytometry results showed that the proportion of CD68<sup>+</sup>/CD11b<sup>+</sup> cells (the source of mononuclear MΦ1 cells) in peripheral blood was significantly higher in BSA-KI<sup>-/+</sup> mice than that in BSA-WT mice; however, in the peripheral blood of, the proportion of CD206<sup>+</sup>/CD11b<sup>+</sup> cells (the source of mononuclear MΦ2 cells) was significantly lower in

BSA-KI<sup>-/+</sup> mice than that in BSA-WT mice significantly (Fig. 8A). qPCR results indicated that KL (Klotho) and *Nfe2l2* (-Nrf2) gene expression level in the peripheral blood cells was significantly lower in BSA-KI<sup>-/+</sup> mice than in BSA-WT mice (Fig. 8B). However, the expression level of inflammation-related genes *Nfkb1* (NFκB) predominate, *Ifng* (IFNγ), *Tnf* (TNFα), and *Il1b* (IL-1β) in peripheral blood cells (MΦ1) in BSA-KI<sup>-/+</sup> mice was significantly higher than those in BSA-WT mice (Fig 8B). Similarly, western blot results indicated the higher expressions of IL-1β and NFκB (p65) and

lower expressions of Klotho and Nrf2 in peripheral blood cells (MΦ1) from BSA-Kl<sup>-/+</sup> mice, which prompts MΦ1 activation (Fig. 8C). These findings suggest that BSA treatment in Kl<sup>-/+</sup> mice activates MΦ1 cells by regulating Nrf2/NF-κB signaling pathways.

### Discussion

The intestine – the main organ of uremic toxin production and discharge [1,4-8,10] – exhibits mechanical, mucous, immune, and biological barriers, which maintain the intestinal tract and the internal environment of the body in a steady state [1,4-8,10]. Among them, the biological barrier is mainly composed of a large number of bacteria, viruses, protozoa, and fungi that parasitize the surface of the intestinal lumen [1, 4-8, 10]. Under normal circumstances, the intestinal microflora and the body are in dynamic equilibrium; when this balance is disrupted, it may damage the function of the

intestinal barrier, leading to a change in the number and proportion of gut bacteria, or translocate them, causing endogenous infection [1,4-8,10]. Some uremic toxins (such as AGE, phenols, indoles and TMAO) have strong biological effects [1,4-8,10]; Mishima and others analyzed the distribution and structure of approximately 190 types of intestinal microorganisms in patients with renal failure and found an imbalance in their abundance; specifically, the abundance of lactic acid bacteria was significantly lower and that of fecal bacteria, *Escherichia coli*, and other microorganisms was significantly higher [40]. An imbalance in the intestinal microecology—a decrease in the number and diversity of intestinal probiotics and an increase in the number and diversity of pathogens—damages the intestinal mucosa barrier, increases the intestinal mucosal permeability, translocates pathogenic bacteria and enterogenous endotoxins into the blood circulation, activates the intestinal mucosal immune system, and induces

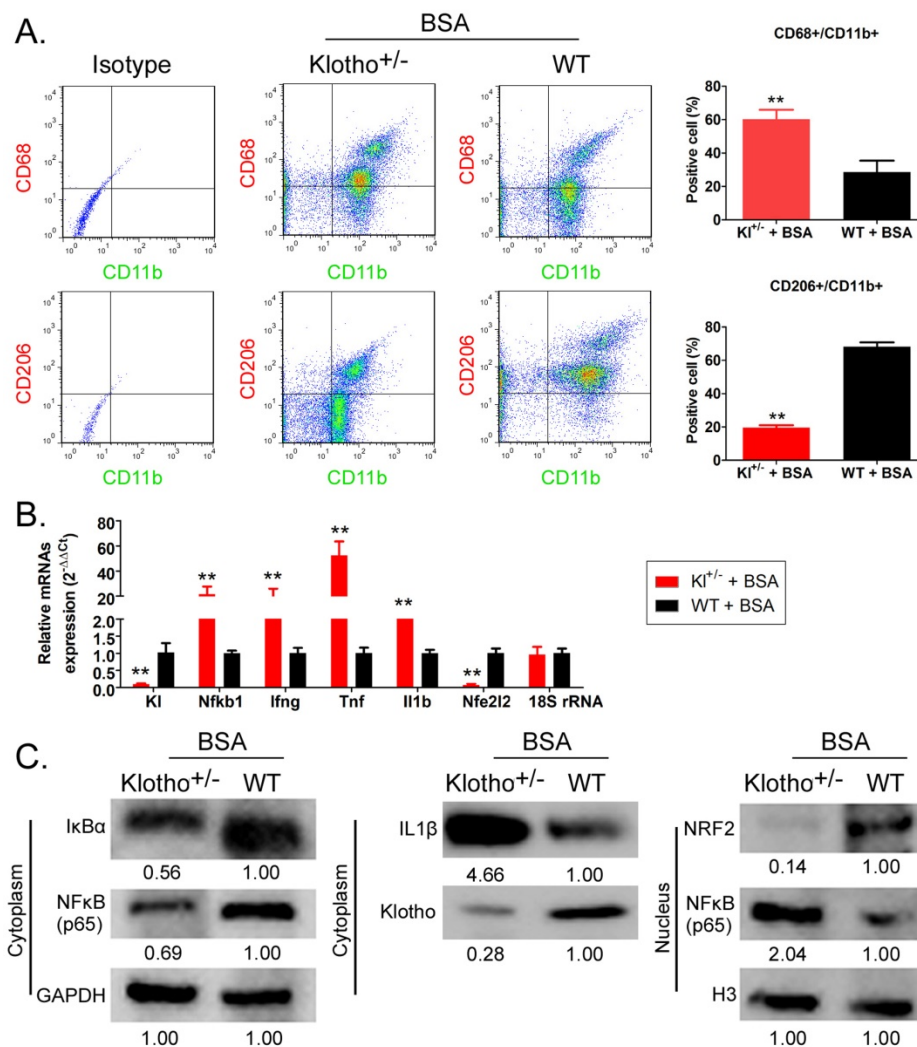


**Figure 8. Bovine serum albumin (BSA) increased the number and activity of MΦ1.** (A) Analysis of the proportion of monocyte-derived macrophage subsets using flow cytometry in BSA-treated Klotho-deficient and wild-type mice. \*\*p < 0.01 (t test); n = 4. (B) qPCR results \*\*p < 0.01 vs WT+BSA; t test; n = 4. (C) Western blot results.

systemic inflammatory reaction, causing kidney damage. The increase in the number of pathogenic bacteria produce urinary toxin, intestinal source of cresol sulfate, sulfuric acid indole phenol, trimethylamine oxide accumulation in the blood, and kidney function impairment and fail to eliminate the toxin, resulting in further kidney damage and function impairment. Whibley and others found that after *Candida albicans* transplantation, the disruption of the intestinal flora in mice induced a significant rise in number of Treg cells, thus disrupting the immune balance.

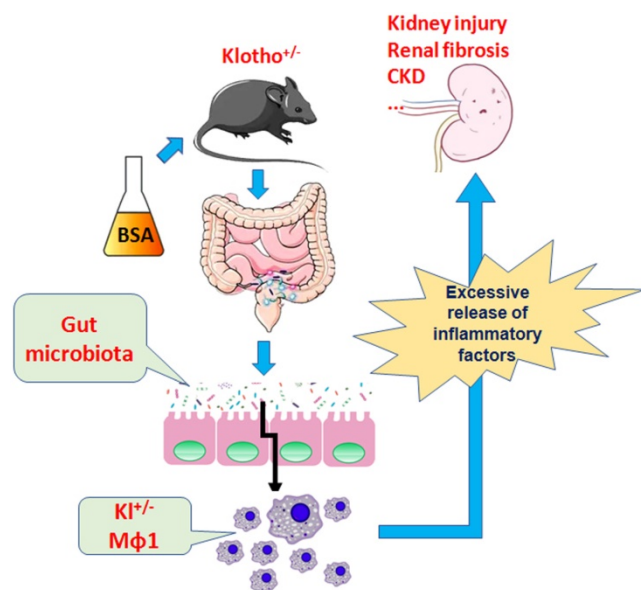


**Figure 9.** BSA aggravates macrophage M1 activation and kidney injury in heterozygous Klotho-deficient mice via the gut microbiota-immune axis.

Simultaneously, an increase in the intestinal pathogenic bacteria activates kidney through its metabolites inside and outside of the macrophage recognition receptors immune response, thus causing kidney damage [41]. Therefore, intestinal dysbiosis causes kidney damage through effects on the immune system, release of urinary toxins, and translocation of pathogenic bacteria translocation [1, 4-8, 10, 40, 41]. The expression of longevity-related genes such as Klotho is also closely associated with renal fibrosis, chronic kidney disease, and immune system imbalance [11, 23, 29, 42 to 45]. Blood vessel endothelial cell aging and atherosclerosis, glomerular fibrosis and kidney damage, and skeletal muscle loss significantly increases the risk of degenerative diseases in Klotho-deficient mice [11,23,29,42 to 45]. In addition, Klotho expression maintains the activity of CD4<sup>+</sup> T cells (Th1), and reduction in Klotho expression significantly induces CD4<sup>+</sup> T cell aging and death [46]. Klotho also promotes Macrophage M1-to-M2 transformation, thus inducing damage

repair [47]. In absence of Klotho expression, an imbalance in FGF23/FGFR/ $\alpha$ -Klotho signaling pathway severely affects the M $\phi$ 1-to-M $\phi$ 2 transformation, leading to an accumulation of inflammatory M $\phi$ 1 cells, eventually inducing damage owing to chronic inflammation [47]. Intestinal dysbiosis and abnormal immune system cause kidney damage and CKD. Therefore, the present study aimed to explore whether there is an association between the intestinal flora, Klotho, and inflammatory cells, especially macrophages and whether they jointly maintain the kidney function and homeostasis.

To answer the above questions, we selected Klotho-deficient heterozygous mice as the research object. We used small doses of BSA (the dose of BSA reported to induce kidney damage in mice is approximately 10-15 mg/g [31], but we selected a dose 1/10 of this dose) to achieve drug-induced kidney injury in mice to investigate whether Klotho mice are more prone to drug-induced kidney damage than WT mice. Histopathological staining and creatinine and urea levels suggest that BSA treatment of Klotho-deficient mice by intraperitoneal gavage causes glomerular fibrosis and mesangial proliferation. The abnormal increase in serum creatinine and urea in Klotho-deficient mice also induce kidney damage; however, the changes were insignificant in WT mice. The results indicate that in absence of Klotho expression in mice, small doses of albumin stimulation for a long time keep burdening the kidney, causing kidney damage.

We also analyzed the distribution, quantity, and community structure of intestinal bacterial flora and the difference in metabolomics in both groups of mice. 16s rRNA v3-v4 sequencing indicated that the intestinal flora of the two groups of mice exhibits significant differences. After long time feeding BSA, the intestinal flora in Klotho-deficient mice treated with BSA for long periods exhibit a significant increase in the relative abundance of microbial species of the genera *Dubosiella*, *Akkermansia*, *Alloprevotella*, *Lachnospiraceae*, and *Muribaculaceae* and significant reduction in the relative abundance of microorganisms belonging to the genus *Allobaculum*.

Microbial diversity and cluster analysis indicated that the number and microbial diversity of the superphylum Patescibacteria, especially the phyla Bacteroidetes and Actinobacteria, decreased and, and the number of microorganisms in the phyla Verrucomicrobia, Acidobacteria, and Tenericutes increased in BSA-treated Klotho-deficient mice. A significant change in the intestinal microecological structure eventually led to a significant change in the metabolites produced by the intestinal

microorganism. In BSA-treated Klotho-deficient mice, metabolic pathways associated with signal transduction, xenobiotics biodegradation and metabolism, lipid metabolism substances were significantly more active than that in the control group; the abundance of proteins involved in signal transduction mechanisms and cell motility also improved significantly. Our previous studies [9, 48] suggest that a change in gut microbial species stimulates the intestinal mucosal barrier and mucosal immune changes, affecting the distribution of intestinal immune cells, immune cells, and peripheral blood and polarity of anomalies.

Stanford and others summarized several reports on the intestinal flora of patients with kidney disease and pointed out that the abundance of several microorganisms (including Enterobacteriaceae and *Streptococcus*) is significantly higher in adult patients with kidney disease, specifically, the difference in the abundance of genus *Lachnospiraceae* was very significant between groups [45]. Moreover, Li and colleagues also reported that the abundance of genera *Lactobacillus*, *Clostridium* IV, *Paraprevotella*, *Clostridium* (sensu stricto), *Desulfovibrio*, and *Alloprevotella* was higher in the fecal samples of patients with chronic kidney disease than that in the healthy control group [46]. The reports are consistent with the findings of our study; this shows that kidney damage induced by BSA intervention and chronic kidney disease in mice is similar to intestinal flora disorder or CKD in humans, and the strain distribution and community structure of intestinal microorganisms is very similar to that in humans. Our findings suggested that in patients with CKD, intestinal microorganisms of the genera *Alloprevotella* and *Lachnospiraceae* are more abundant. Imbalance of intestinal flora will accompany the immune system and inflammatory cells proportion of exceptions, the more has been written. The results also suggest that BSA treatment in mice increases the number of macrophages, especially M $\Phi$ 1. However, BSA-treated Klotho-deficient mice showed a disrupted ratio of peripheral blood M $\Phi$ 1 and M $\Phi$ 2; the number of M $\Phi$ 1 continued to increase, and that of M $\Phi$ 2 continued to decline. This finding suggests that Klotho deficiency induces persistent inflammation (M $\Phi$ 1 cause inflammation), and significantly impairs the tissue repair ability (M $\Phi$ 2 have tissue repair function). BSA-treated Klotho-deficient mice also showed higher expression of NF $\kappa$ B (p65) and lower expression of Nrf2 protein in M $\Phi$ 1 cells, prompting M $\Phi$ 1 activation. This result is consistent with previously reported findings [51].

Therefore, the present study demonstrates that BSA alters the community structure of the intestinal flora and induces kidney damage and chronic kidney

disease in mice and promotes immune activation and chronic inflammation in Klotho-deficient mice with intestinal dysbacteriosis (Fig 9). Changes in the number of immune cells, especially the source of mononuclear macrophages and imbalance in the expression of proteins in the Nrf2/NF $\kappa$ B signaling pathway lead to increased inflammation and kidney damage.

## Supplementary Material

Supplementary figures and tables.

<http://www.ijbs.com/v17p0742s1.pdf>

## Acknowledgements

This work was supported by the National Natural Science Foundation of China (grant no. 82070762, 81973899) and National Key R&D Program of China (2018YFC1704300). We declared no potential conflicts of interest.

## Competing Interests

The authors have declared that no competing interest exists.

## References

1. Yang T, Richards EM, Pepine CJ, Raizada MK. The gut microbiota and the brain-gut-kidney axis in hypertension and chronic kidney disease. *Nat Rev Nephrol.* 2018; 14: 442-56.
2. Jha V, Garcia-Garcia G, Iseki K, Li Z, Naicker S, Plattner B, et al. Chronic kidney disease: global dimension and perspectives. *Lancet.* 2013; 382: 260-72.
3. Pluznick JL. The gut microbiota in kidney disease. *Science.* 2020; 369: 1426-7.
4. Antza C, Stabouli S, Kotsis V. Gut microbiota in kidney disease and hypertension. *Pharmacol Res.* 2018; 130: 198-203.
5. Onal EM, Afsar B, Covic A, Vaziri ND, Kanbay M. Gut microbiota and inflammation in chronic kidney disease and their roles in the development of cardiovascular disease. *Hypertens Res.* 2019; 42: 123-40.
6. Cigarran Guldris S, Gonzalez Parra E, Cases Amenos A. Gut microbiota in chronic kidney disease. *Nefrologia.* 2017; 37: 9-19.
7. Shi K, Wang F, Jiang H, Liu H, Wei M, Wang Z, et al. Gut bacterial translocation may aggravate microinflammation in hemodialysis patients. *Dig Dis Sci.* 2014; 59: 2109-17.
8. Tang WH, Kitai T, Hazen SL. Gut Microbiota in Cardiovascular Health and Disease. *Circ Res.* 2017; 120: 1183-96.
9. Liu J, Lai L, Lin J, Zheng J, Nie X, Zhu X, et al. Ranitidine and finasteride inhibit the synthesis and release of trimethylamine N-oxide and mitigates its cardiovascular and renal damage through modulating gut microbiota. *Int J Biol Sci.* 2020; 16: 790-802.
10. Wang Y, Li J, Chen C, Lu J, Yu J, Xu X, et al. Targeting the gut microbial metabolic pathway with small molecules decreases uremic toxin production. *Gut Microbes.* 2020; 12: 1-19.
11. Kuro-o M, Matsumura Y, Aizawa H, Kawaguchi H, Suga T, Utsugi T, et al. Mutation of the mouse klotho gene leads to a syndrome resembling ageing. *Nature.* 1997; 390: 45-51.
12. Urakawa I, Yamazaki Y, Shimada T, Iijima K, Hasegawa H, Okawa K, et al. Klotho converts canonical FGF receptor into a specific receptor for FGF23. *Nature.* 2006; 444: 770-4.
13. Xu Y, Sun Z. Molecular basis of Klotho: from gene to function in aging. *Endocr Rev.* 2015; 36: 174-93.
14. Bian A, Neyra JA, Zhan M, Hu MC. Klotho, stem cells, and aging. *Clin Interv Aging.* 2015; 10: 1233-43.
15. Chen G, Liu Y, Goetz R, Fu L, Jayaraman S, Hu MC, et al. alpha-Klotho is a non-enzymatic molecular scaffold for FGF23 hormone signalling. *Nature.* 2018; 553: 461-6.
16. Gao D, Wang S, Lin Y, Sun Z. *In vivo* AAV delivery of glutathione reductase gene attenuates anti-aging gene klotho deficiency-induced kidney damage. *Redox Biol.* 2020; 37: 101692.
17. Gazdhar A, Ravikumar P, Pastor J, Heller M, Ye J, Zhang J, et al. Alpha-Klotho Enrichment in Induced Pluripotent Stem Cell Secretome Contributes to Antioxidative Protection in Acute Lung Injury. *Stem Cells.* 2018; 36: 616-25.

18. Qian Y, Guo X, Che L, Guan X, Wu B, Lu R, et al. Klotho Reduces Necroptosis by Targeting Oxidative Stress Involved in Renal Ischemic-Reperfusion Injury. *Cell Physiol Biochem*. 2018; 45: 2268-82.
19. Kimura T, Shiizaki K, Kurosu H, Akimoto T, Shinzato T, Shimizu T, et al. The impact of preserved Klotho gene expression on anti-oxidative stress activity in healthy kidney. *Am J Physiol Renal Physiol*. 2018.
20. Chen K, Sun Z. Activation of DNA demethylases attenuates aging-associated arterial stiffening and hypertension. *Aging Cell*. 2018: e12762.
21. Minamizaki T, Konishi Y, Sakurai K, Yoshioka H, Aubin JE, Kozai K, et al. Soluble Klotho causes hypomineralization in Klotho-deficient mice. *J Endocrinol*. 2018; 237: 285-300.
22. Chuchana P, Mausset-Bonnefont AL, Mathieu M, Espinoza F, Teigell M, Toupet K, et al. Secreted alpha-Klotho maintains cartilage tissue homeostasis by repressing NOS2 and ZIP8-MMP13 catabolic axis. *Aging (Albany NY)*. 2018; 10: 1442-53.
23. Sato S, Kawamata Y, Takahashi A, Imai Y, Hanyu A, Okuma A, et al. Ablation of the p16(INK4a) tumour suppressor reverses ageing phenotypes of klotho mice. *Nat Commun*. 2015; 6: 7035.
24. Lee S, Choi J, Mohanty J, Sousa LP, Tome F, Pardon E, et al. Structures of beta-klotho reveal a 'zip code'-like mechanism for endocrine FGF signalling. *Nature*. 2018; 553: 501-5.
25. Manou E, Thodis E, Arsos G, Pasadakis P, Panagoutsos S, Papadopoulou D, et al. Fibroblast Growth Factor 23 and alpha-Klotho Protein Are Associated with Adverse Clinical Outcomes in Non-Dialysis CKD Patients. *Kidney Blood Press Res*. 2020; p: 1-16.
26. Maique J, Flores B, Shi M, Shepard S, Zhou Z, Yan S, et al. High Phosphate Induces and Klotho Attenuates Kidney Epithelial Senescence and Fibrosis. *Front Pharmacol*. 2020; 11: 1273.
27. Chen F, Gao Q, Wei A, Chen X, Shi Y, Wang H, et al. Histone deacetylase 3 aberration inhibits Klotho transcription and promotes renal fibrosis. *Cell Death Differ*. 2020.
28. Lee J, Tsogbadrakh B, Yang S, Ryu H, Kang E, Kang M, et al. Klotho ameliorates diabetic nephropathy via LKB1-AMPK-PGC1alpha-mediated renal mitochondrial protection. *Biochem Biophys Res Commun*. 2020.
29. Lv J, Chen J, Wang M, Yan F. Klotho alleviates indoxyl sulfate-induced heart failure and kidney damage by promoting M2 macrophage polarization. *Aging (Albany NY)*. 2020; 12: 9139-50.
30. Zhang H, Zhou L, Yuen J, Birkner N, Leppert V, O'Day PA, et al. Delayed Nrf2-regulated antioxidant gene induction in response to silica nanoparticles. *Free Radic Biol Med*. 2017; 108: 311-9.
31. Lu MC, Zhao J, Liu YT, Liu T, Tao MM, You QD, et al. CPUY192018, a potent inhibitor of the Keap1-Nrf2 protein-protein interaction, alleviates renal inflammation in mice by restricting oxidative stress and NF-kappaB activation. *Redox Biol*. 2019; 26: 101266.
32. Oeckinghaus A, Ghosh S. The NF-kappaB family of transcription factors and its regulation. *Cold Spring Harb Perspect Biol*. 2009; 1: a000034.
33. Ghosh S, Choudhury S, Chowdhury O, Mukherjee S, Das A, Sain A, et al. Inflammation-induced behavioral changes is driven by alterations in Nrf2-dependent apoptosis and autophagy in mouse hippocampus: Role of fluoxetine. *Cell Signal*. 2020; 68: 109521.
34. Kohler UA, Bohm F, Rolfs F, Egger M, Hornemann T, Pasparakis M, et al. NF-kappaB/RelA and Nrf2 cooperate to maintain hepatocyte integrity and to prevent development of hepatocellular adenoma. *J Hepatol*. 2016; 64: 94-102.
35. Liu T, Liu Y, Huang Y, Chen J, Yu Z, Chen C, et al. miR-15b induces premature ovarian failure in mice via inhibition of alpha-Klotho expression in ovarian granulosa cells. *Free Radic Biol Med*. 2019; 141: 383-92.
36. Cassis P, Locatelli M, Cerullo D, Corna D, Buelli S, Zanchi C, et al. SGLT2 inhibitor dapagliflozin limits podocyte damage in proteinuric nondiabetic nephropathy. *JCI Insight*. 2018; 3.
37. Xu P, Wang J, Hong F, Wang S, Jin X, Xue T, et al. Melatonin prevents obesity through modulation of gut microbiota in mice. *J Pineal Res*. 2017; 62.
38. Ji ZH, Ren WZ, Gao W, Hao Y, Gao W, Chen J, et al. Analyzing the innate immunity of NIH hairless mice and the impact of gut microbial polymorphisms on *Listeria monocytogenes* infection. *Oncotarget*. 2017; 8: 106222-32.
39. Caporaso JG, Kuczynski J, Stombaugh J, Bittinger K, Bushman FD, Costello EK, et al. QIIME allows analysis of high-throughput community sequencing data. *Nat Methods*. 2010; 7: 335-6.
40. Edgar RC. Search and clustering orders of magnitude faster than BLAST. *Bioinformatics*. 2010; 26: 2460-1.
41. Sakaki T, Takeshima T, Tominaga M, Hashimoto H, Kawaguchi S. Recurrence of ICA-PCoA aneurysms after neck clipping. *J Neurosurg*. 1994; 80: 58-63.
42. Looft T, Johnson TA, Allen HK, Bayles DO, Alt DP, Stedtfeld RD, et al. In-feed antibiotic effects on the swine intestinal microbiome. *Proc Natl Acad Sci U S A*. 2012; 109: 1691-6.
43. Segata N, Izard J, Waldron L, Gevers D, Miropolsky L, Garrett WS, et al. Metagenomic biomarker discovery and explanation. *Genome Biol*. 2011; 12: R60.
44. Parks DH, Tyson GW, Hugenholtz P, Beiko RG. STAMP: statistical analysis of taxonomic and functional profiles. *Bioinformatics*. 2014; 30: 3123-4.
45. Stanford J, Charlton K, Stefoska-Needham A, Ibrahim R, Lambert K. The gut microbiota profile of adults with kidney disease and kidney stones: a systematic review of the literature. *BMC Nephrol*. 2020; 21: 215.
46. Li F, Wang M, Wang J, Li R, Zhang Y. Alterations to the Gut Microbiota and Their Correlation With Inflammatory Factors in Chronic Kidney Disease. *Front Cell Infect Microbiol*. 2019; 9: 206.
47. Fitzpatrick EA, Han X, Xiao Z, Quarles LD. Role of Fibroblast Growth Factor-23 in Innate Immune Responses. *Front Endocrinol (Lausanne)*. 2018; 9: 320.
48. Lin J, Nie X, Xiong Y, Gong Z, Chen J, Chen C, et al. Fisetin regulates gut microbiota to decrease CCR9(+)/CXCR3(+)/CD4(+) T-lymphocyte count and IL-12 secretion to alleviate premature ovarian failure in mice. *Am J Transl Res*. 2020; 12: 203-47.
49. Stanford J, Charlton K, Stefoska-Needham A, Ibrahim R, Lambert K. The gut microbiota profile of adults with kidney disease and kidney stones: a systematic review of the literature. *BMC Nephrol*. 2020; 21: 215.
50. Li F, Wang M, Wang J, Li R, Zhang Y. Alterations to the Gut Microbiota and Their Correlation With Inflammatory Factors in Chronic Kidney Disease. *Front Cell Infect Microbiol*. 2019; 9: 206.
51. Yu Y, He J, Li S, Song L, Guo X, Yao W, et al. Fibroblast growth factor 21 (FGF21) inhibits macrophage-mediated inflammation by activating Nrf2 and suppressing the NF-kappaB signaling pathway. *International immunopharmacology*. 2016; 38: 144-52.